Science of the Total Environment 846 (2022) 157290

Contents lists available at ScienceDirect

Science of the Total Environment

journal homepage: www.elsevier.com/locate/scitotenv

Characterization of odour emissions in a wastewater treatment plant using a drone-based chemical sensor system

Javier Burgués [a,b], Silvia Doñate [c], María Deseada Esclapez [c], Lidia Saúco [c], Santiago Marco [a,b,*]

[a] Institute for Bioengineering of Catalonia (IBEC), The Barcelona Institute of Science and Technology, Baldiri Reixac 10-12, 08028 Barcelona, Spain
[b] Department of Electronics and Biomedical Engineering, Universitat de Barcelona, Marti i Franqués 1, 08028 Barcelona, Spain
[c] Depuración de Aguas del Mediterráneo (DAM), Avenida Benjamín Franklin 21, Parque Tecnológico, Paterna 46980, Spain

HIGHLIGHTS

- A drone-based system for the prediction of odour concentration is described.
- The prototype is demonstrated and validated in a wastewater treatment plant.
- The accuracy of the odour predictions is benchmarked against dynamic olfactometry.
- Interpolated odour concentration map reveals main odour hotspots.

GRAPHICAL ABSTRACT

ARTICLE INFO

Editor: Damià Barceló

Keywords:
Environmental monitoring
Electronic nose
Chemical sensors
Drone
Olfaction
Calibration
Odour quantification
Dynamic olfactometry
WWTP

ABSTRACT

Conventionally, odours emitted by different sources present in wastewater treatment plants (WWTPs) are measured by dynamic olfactometry, where a human panel sniffs and analyzes air bags collected from the plant. Although the method is considered the gold standard, the process is costly, slow, and infrequent, which does not allow operators to quickly identify and respond to problems. To better monitor and map WWTP odour emissions, here we propose a small rotary-wing drone equipped with a lightweight (1.3-kg) electronic nose. The "sniffing drone" sucks in air via a ten-meter (33-foot) tube and delivers it to a sensor chamber where it is analyzed in real-time by an array of 21 gas sensors. From the sensor signals, machine learning (ML) algorithms predict the odour concentration that a human panel using the EN13725 methodology would report. To calibrate and validate the predictive models, the drone also carries a remotely controlled sampling device (compliant with EN13725:2022) to collect sample air in bags for post-flight dynamic olfactometry. The feasibility of the proposed system is assessed in a WWTP in Spain through several measurement campaigns covering diverse operating regimes of the plant and meteorological conditions. We demonstrate that training the ML algorithms with dynamic (transient) sensor signals measured in flight conditions leads to better performance than the traditional approach of using steady-state signals measured in the lab via controlled exposures to odour bags. The comparison of the electronic nose predictions with dynamic olfactometry measurements indicates a negligible bias between the two measurement techniques and 95 % limits of agreement within a factor of four. This apparently large disagreement, partly caused by the high uncertainty of olfactometric measurements (typically a factor of two), is more than offset by the immediacy of the predictions and the practical advantages of using a drone-based system.

* Corresponding author at: Department of Electronics and Biomedical Engineering, Universitat de Barcelona, Marti i Franqués 1, 08028 Barcelona, Spain.
E-mail address: santiago.marco@ub.edu (S. Marco).

http://dx.doi.org/10.1016/j.scitotenv.2022.157290
Received 25 February 2022Received in revised form 4 July 2022Accepted 7 July 2022
Available online 14 July 2022

1. Introduction

Odour monitoring is routinely performed in wastewater treatment plants (WWTPs) to verify the efficiency of odour abatement systems (Munoz et al., 2010), identify fugitive emissions within the plant (Zarra et al., 2008), and predict and minimize off-site odour impact (Naddeo et al., 2012; Stuetz and Frechen, 2001). Even when present at low concentrations, unpleasant odorous compounds featuring very low olfactory threshold can induce significant discomfort in residents of neighbouring areas. Additionally, a variety of health effects have been associated with exposure to odorous compounds in plant employees(Martí et al., 2014). These health effects include headaches, nausea, vomiting, dizziness, and eye and respiratory irritation. The perception of unpleasant smells is a form of indication of potential human health risks (Carrera-Chapela et al., 2014), and some authors have reported a significant correlation between odour concentration and the health hazard index (HI) (Byliński et al., 2019).

Currently, quantitative and qualitative characterization of odours can only be properly assessed via standardized protocols involving human panels (e.g., dynamic olfactometry as per standard EN13725:2022) ("EN13725: Stationary source emissions - Determination of odour concentration by dynamic olfactometry and odour emission rate," 2022). The main practical issue with these methodologies is the high cost and discontinuity of each measurement, as samples must be collected on site and analyzed in a certified laboratory. This leads to infrequent and spatially sparse measurements that are insufficient to characterize odour emissions in a complex plant.

It has been long recognized that wastewater treatment plants emit a large number of odorous compounds including (not exhaustive) Hydrogen sulfide, organic sulfur compounds, aldehydes and ketones, ammonia and amines and chlorinated VOCs. While these compounds are present in most odour emissions, their relative concentration and contribution to the final odour perception will widely vary across sites, water influx quality, processes, etc. Several studies have found that while H_2S concentration is a good marker of the overall odour concentration the correlations are only moderate: in the range 0.3 to 0.7 (Stuetz and Frechen, 2001; Devai and DeLaune, 1999; Dincer and Muezzinoglu, 2008; Sivret et al., 2016). This suggests that the inclusion of additional chemical sensors and proper data processing may be necessary to improve the final prediction of the odour concentration.

Instrumental Odour Monitoring Systems (IOMS) or, more colloquially, electronic noses (e-noses) are currently the most promising instruments to quantify and classify odours (Bax et al., 2020). Electronic noses deployed in fixed locations within WWTPs, landfills, ports, composting plants, farms and petrochemical plants, among others, have obtained promising results for odour classification and quantification (Capelli et al., 2014; Staerz et al., 2020). While static e-noses are perfect for monitoring specific points of an industrial plant with high temporal resolution, the highly localized information provided by these units is not sufficient for characterizing odour events in a complex site with multiple foci, such as WWTPs. Not only because of the high number of potential emission sources but also because many of these sources are area sources (e.g., buffer tank domes, bioreactors, anaerobic digesters, settlers) that are difficult to access or monitor from a single location. A proper spatial coverage with fixed measurements would require the deployment of many instruments within a potentially vast area, which is infeasible due to the high acquisition and maintenance costs of each unit (Schwarzböck, 2012).

IOMS are today the object of an intense standardization effort within CEN TC264/WG41. While no standard has been officially issued, these systems provide predictions of odour concentration that can be directly compared to the values obtained by dynamic olfactometry according to EN13725 (same scale). Today, ouE/m^3 is reserved for olfactometric evaluations carried out according to EN13725 methodology. The use of such units for IOMS predictions in not yet accepted, indicating that IOMS is a surrogate method that cannot fully replace EN13725 evaluations. However, since both evaluations are in the same scale, we will use the term predicted odour concentration in equivalent ouE/m^3.

A promising approach for obtaining spatially dense odour measurements in WWTPs (and other industrial sites) is the use of a drone-mounted electronic nose. Despite the application of drones for environmental chemical sensing has grown exponentially in the last decade (Burgués and Marco, 2020), their use for odour monitoring has been largely ignored. Current state of the art mostly focuses on the measurement of greenhouse gases (e.g., CH_4, CO_2) or in indoor experiments using nano-drones (Burgués et al., 2019; Duisterhof et al., 2021; Shigaki et al., 2018). Only very recently the suitability of small drones (<10 kg) for odour monitoring has been assessed in WWTPs (Burgués et al., 2021b) and oil refinery plants (Serta et al., 2021) using commercial drones equipped with electrochemical sensors for odorous compounds such as hydrogen sulfide (H_2S) or ammonia (NH_3). To bypass the "downwash" problem (air disturbance created by the drone's propellers that can affect gas concentration measurements), the sensors were either suspended at a safe distance underneath the drone via a 4-m cable (Serta et al., 2021) or connected to a pumped system with a 10-m sampling tube (Burgués et al., 2021b). While these two preliminary works represent an important first step in assessing the feasibility of drones for measuring odours, it is well known that measuring odour concentration (as humans perceive it) is much more complex than measuring the concentration of individual gases (Thomas-Danguin et al., 2014). A formidable challenge is to obtain electronic nose based odour concentration estimation systems that could model these interactions (Yan et al., 2017; Hudon et al., 2000; Szulczyński et al., 2017).

In this paper we present a drone equipped with an electronic nose able to predict the odour concentration of WWTP emission sources with moderate correlation to dynamic olfactometry results (ouE/m^3) and provide spatially dense maps of predicted odour concentration. The core of the SNIFFDRONE prototype is an electronic nose recently developed by our research group as a payload for commercial drones (Burgués et al., 2021a, 2021b; Burgués et al., 2021c; Burgués et al., 2020). The 1.3-kg (2.9-lb) instrument, which was initially calibrated and validated in the laboratory via controlled exposures to odour bags collected on a test WWTP, achieved a 72 % correlation with dynamic olfactometry when mounted on a small rotary-wing drone during preliminary field measurements in the same WWTP. This correlation level was obtained with 13 blind samples spanning the range 100–7000 ouE/m^3. One main question we want to address in the present work is if this field performance can be improved by calibrating the instrument with transient sensor signals measured in flight conditions (dynamic calibration) rather than with steady-state sensor signals measured in the lab (static calibration). Fig. 1 illustrates this concept. Dynamic calibration has the theoretical advantage that the signals used for calibration and operation of the instrument are exactly of the same nature, potentially leading to a better performance than static calibration. However, a priori it is not trivial how to build a predictive model using fluctuating sensor signals.

The SNIFFDRONE proposal goes beyond the state of the art in several aspects (Table 1). Instead of monitoring single gases like existing drone-based systems, SNIFFDRONE analyzes the odour mixtures as a whole using an array of 21 chemical sensors and machine learning (ML) algorithms. A remotely controlled odour sampling device installed on the drone provides ground truth for the calibration and validation of the predictive models in operational conditions. Second, while current environmental drones use univariate calibration models to convert individual sensor signals into concentration units (e.g., parts-per-million), SNIFFDRONE uses multivariate calibration models to convert time-varying patterns of sensor array signals into odour concentration units (ou_E/m^3). Third, to best of our knowledge odour mapping and source localization using drones has not been accomplished or even attempted in realistic scenarios such as WTTPs. Here we will show for the first time the complexity of this type of operating conditions by flying over a WWTP for model development and validation, including four full days of plant monitoring in different operating and meteorological conditions.

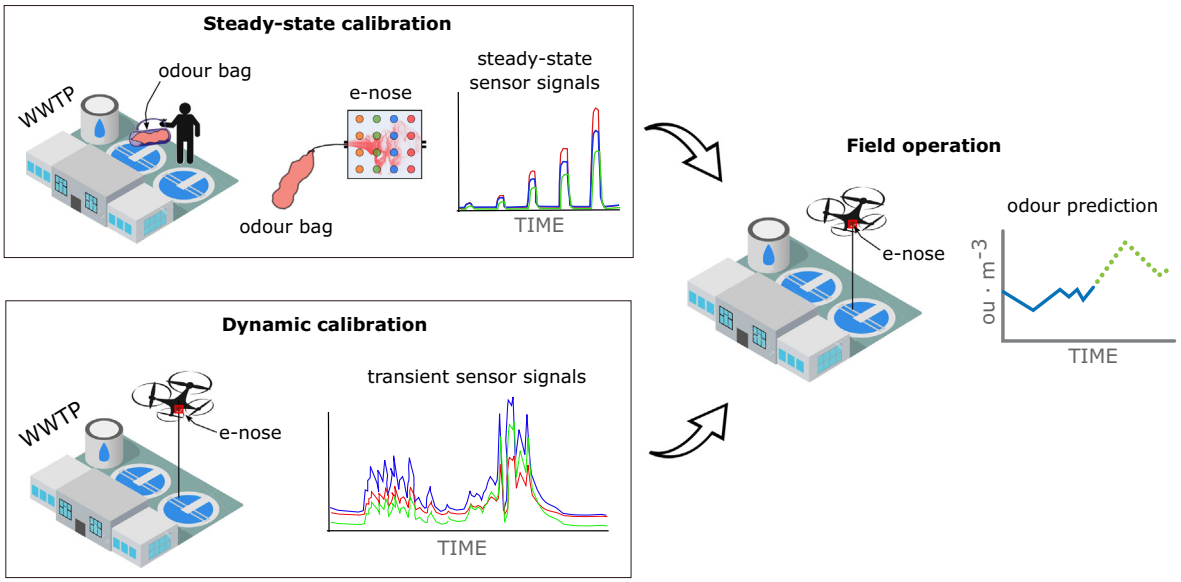

Fig. 1. Diagram illustrating two calibration methodologies (steady-state vs dynamic calibration) for an electronic nose used for real-time odour measurements in a WWTP. Steady-state calibration leads to more robust models, however signals measured in the field are of transient nature. Dynamic calibration uses transient signals to build the calibration model, so it can potentially lead to better field performance.

2. Materials and methods

2.1. Drone and payload

The prototype built in this project uses the DJI M600 rotary-wing drone (DJI International, China) and a custom payload (Fig. 2) consisting of the RHINOS e-nose (Burgués et al., 2021a, 2021b, 2021c) and an odour sampling device compliant with EN13725 standard (Olfasense GmbH, Germany). The latter is used to collect odour bags for post-flight dynamic olfactometry, which enables the calibration and validation of the IOMS predictive models in operational conditions. A custom support was designed to attach both instruments underneath the drone without affecting its center of mass and preventing any collision during take-off or landing. The e-nose and the sampler have their own dedicated sampling system. In both cases, aspiration of the sample is achieved by vacuum pumps and PTFE tubing of 10-m length connected to the inlet of the instruments. The open ends of both tubes are tied together to ensure sampling from the exact same location. In this way, the contents of the sampling bag are a mirror of the gas composition reaching the sensing chamber, so that the e-nose signals and the dynamic olfactometry measurements can be properly compared. A plumb bob of 150 g is attached to the end of the tubing to keep them as straight as possible during flight and reduce oscillations due to wind. The chosen length of the tubing allows that in flight conditions the sample is taken from a region underneath the drone not disturbed by the propellers' downwash. It should be made clear that the e-nose does not analyze the contents of the bag, but the sample aspirated through its dedicated tube.

Table 1
Comparison of SNIFFDRONE with state-of-the-art environmental drones (Serta et al., 2021; Burgués and Marco, 2020; Sassi et al., 2018).

	State of the art	SNIFFDRONE
Sensing system	Electrochemical sensors for H_2S, NH_3, SO_2, …	Hybrid electronic nose with 21 chemical sensors (MOX, EC, NDIR)
Signal / data processing	Measurement of single gases (ppm)	Estimation of odour concentration (ou_E/m^3)
Calibration model	Univariate calibration	Multivariate predictive models
Calibration conditions	In the laboratory	In the field

This allows it to work regardless of the presence of the sampler. The delay in the sample transport through the tubing (~5 s) was used by the e-nose firmware to synchronize the sensor measurements with the GPS position. The total weight of the payload including the mounting plate and the tubing is ~6.2 kg.

The RHINOS e-nose is a lightweight (~1.3 kg) and portable e-nose designed for real-time monitoring of WWTP odours. It contains all the necessary elements required for stand-alone operation (i.e., battery, GPS,

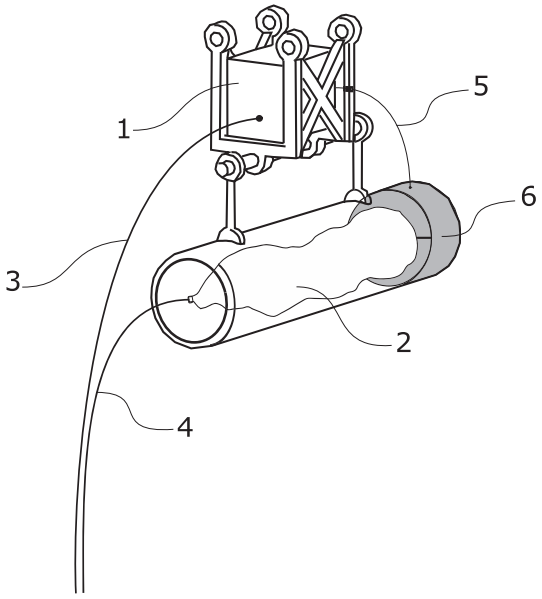

Fig. 2. Schematic illustration of the payload. The payload consists of the RHINOS e-nose (1) and an odour sampling device compliant with EN13725 standard (2). Two independent tubes of 10 m length are used to deliver sample air to the on-board instruments while avoiding the downwash of the drone (3, 4). A wired connection between the e-nose and the odour sampler allows its remote activation from the ground station (5). The battery and vacuum pump of the odour sampler are located in the back side of the instrument (6).

radio link, microcontroller, datalogger, etc.). The core of the system is an array of 21 chemical sensors, including 16 metal oxide (MOX) sensors with broadband sensitivity to different VOCs, 4 electrochemical cells for H_2S, NH_3, SO_2 and CO, and 1 non-dispersive infrared (NDIR) sensor for CO_2. Additional sensors for temperature, humidity, pressure, and flow rate are also included. All these sensors (except the flow rate sensor) are hosted in a miniaturized sensing chamber (91 cm^3 internal volume) driven by a vacuum micropump with high flow rate (1.8 L/min), ensuring a filling time of ~10 s. Due to the high-power dissipation of the MOX sensors, the temperature and relative humidity inside the sensing chamber are relatively stable. For example, in our field experiments at ambient temperatures between 24 and 34 °C and relative humidity between 30 and 55 % r.h. (see Appendix A.2), the temperature and humidity inside the sensing chamber remained at 54 ± 2 °C and 10 ± 2.5 % r.h., respectively. The measured sensor signals and GPS data are transmitted every 6 s to a base station using a ZigBee radio link. A detailed description and characterization of the e-nose is provided elsewhere (Burgués et al., 2021a, 2021b, 2021c).

The odour sampling device (Olfasense GmbH, Germany) is made with a sealed PVC container with capacity for 10-litre gas sampling bags. A powerful vacuum pump (10 L/min) integrated in the device evacuates the container in ~1 min, filling the bag with the odour sample. Although this device is designed as a hand-held unit that must be activated manually via a button on its handle, we modified it to allow its activation via a digital signal. This allowed us to remotely control the activation of the device by simply sending a command from the base station to the e-nose.

2.2. Test site and data collection

A medium-sized WWTP with an extension of 35,000 m^2 and located in the south of Spain was used for field measurements (Fig. 3). The immediate surroundings of the WWTP are farmland and a natural area, being the closest residential area at a distance of 4.5 km. Due to its location, approximately 30 % of the input flow has an industrial origin, mainly manufactured products from the agri-food sector, with noteworthy activity of the canning industry. Its architecture includes a preliminary treatment, a double-stage secondary treatment composed by two bioreactors and two settlers in cascade, a tertiary treatment, and a dedicated sludge line. Air tanks are open air. The plant is designed to treat an input flow of 25.000 m^3/day, however the average flow is of 18.279 m^3/day. The plant design could provide service to a total of 292.000 inhabitants. The outward flow rate of the chemical deodorization system is 20.000 m^3/h. The total emission surface of the settlers and bioreactors is 1080 m^2 and 440 m^2, respectively. *The* deodorisation strategy of the plant included a wet scrubbing system that filters the fumes from different parts of the plant with a two-phase system involving NaClO and NaOH scrubbing (González-Sánchez et al., 2008). The filtered air is released to the atmosphere through an exhaust chimney located on the ceiling of the sludge dehydration building.

Two measurement campaigns were carried out in the summer season, when odour-related problems are exacerbated by the high ambient temperatures. Within each campaign, measurements were performed in two consecutive days to capture different operating and weather conditions (see sections A.1 and A.2 of the Appendix). A total of 73 measurements were completed at the end of the two campaigns (42 odour measurements + 31 blank samples). The odour measurements were focused around the four most problematic odour sources (according to the plant operators): (1) pretreatment building, (2) settlers, (3) bioreactors, and (4) deodorisation chimney. Each source was sampled from various heights (1–6 m distance between the inlet of the sampling tube and the surface of the emission source) to capture a wide range of odour concentrations. Blank measurements were performed in the perimeter of the plant with the inlet of the system at 10 cm from the ground. Under these conditions no odour from the WWTP was perceivable by the members of the team and the sensors were able to recover their baseline level. These blank measurements will be used to assess the baseline drift of the sensors between measurement campaigns, and eventually compensate it during data analysis. Table 2 summarizes the measurement plan.

To perform an odour measurement, the drone is flown to the desired measurement location where it is kept hovering for approximately 5 min (Fig. 4). During this process, the IOMS is measuring continuously to capture a sufficiently long time series of sensor signals that would allow us to assess the variability of the emissions from the studied source. In the middle of the hovering period (t = 2 min), the sampling device on the drone is remotely activated for 1 min to capture an odour sample into the 10-L Nalophan bag. At the end of the hovering period (t = 5 min), the drone is landed in a convenient location to remove the odour bag from the sampling device and replace it with a new one. The odour bags removed from the drone are stored in an opaque container and sent to a certified laboratory where they are analyzed by dynamic olfactometry in <30 h, complying with EN13725 standard. Dynamic olfactometry is carried out using a T08 olfactometer (Odournet GmbH) configured with the "yes/no" method and four panelists.

The maximum allowable confidence interval according to EN13725 ("EN13725: Stationary source emissions - Determination of odour concentration by dynamic olfactometry and odour emission rate," 2022) for a single measurement value with a coverage factor of k = 2 is $x/2.21 < x < 2.21$, based on the intermediate precision value (expressed as repeatability, r) of 0.477. Regarding the accuracy of the odour concentration measurement (A_{od}), the standard defines a limit of 0.217. Based on the most

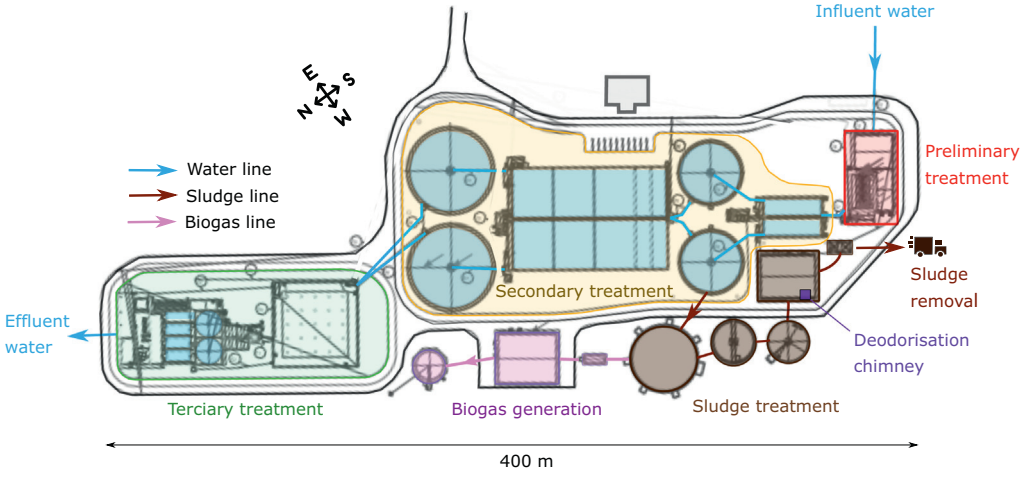

Fig. 3. Schematic representation of the WWTP of Molina de Segura (Murcia, Spain).

Table 2
Number of samples collected in each source during the four measurement days.

Day	Date	Settler	Bioreactor	Pretreatment	Chimney	Total (odour)	Blanks	Total
1	24/06/2020	3	3	2	2	10	7	17
2	25/06/2020	2	2	2	2	8	6	14
3	14/07/2020	3	3	3	3	12	11	23
4	15/07/2020	3	3	3	3	12	7	19
Total		11	11	10	10	42	31	73

recent n = 12 measurements of the reference gas n-butanol, included during the measurement session, the accuracy A_{od} and the intermediate precision value r met the EN13725 criteria mentioned above. This implies that the actual confidence interval in the olfactometry laboratory for a single measurement value x, including predilution, is within the range stated above. It is assumed that this uncertainty and precision, based on verification with reference gases, are transferable to environmental samples.

2.3. Electronic nose calibration and validation

2.3.1. Signal pre-processing

The goals of signal pre-processing are to improve the signal-to-noise ratio (SNR) of some sensors, remove measurement artifacts (e.g., spikes) and correct the drift of the sensors baseline. Not all sensors required the same pre-processing. For example, MOX sensor signals showed periodic spikes that we filtered out with a median filter (window size = 3 samples). Electrochemical sensors were more affected by baseline drift, which we noticed by looking at the reference blank samples captured at the beginning of each measurement campaign. To correct this drift, we subtracted an offset from each sensor response to ensure that the baseline at the beginning of the measurement campaign matches the reference background levels of the target gases (see Appendix A.3). We did not check for any potential drift in sensitivity.

2.3.2. PLS modelling

Partial least squares (PLS) regression (Wold et al., 2001) was chosen to predict the odour concentration $\boldsymbol{y}$ ($n \times 1$) based on the features $\boldsymbol{X}$ ($n \times m$) extracted from the sensor signals, where n is the number of samples and m is the number of features. PLS is particularly well suited for datasets where $m > n$,i.e. the matrix $\boldsymbol{X}$ has more predictors (columns) than observations (rows), and there is multicollinearity among the features in $\boldsymbol{X}$ (Mehmood et al., 2012). The PLS model equation is as follows:

$$\boldsymbol{y} = \boldsymbol{X\beta} + \boldsymbol{e} \quad (1)$$

where $\boldsymbol{\beta}$ ($m \times 1$) is the vector of regression coefficients and $\boldsymbol{e}$ ($n \times 1$) is the residual error. The matrices $\boldsymbol{X}$ and $\boldsymbol{y}$ are logarithmically transformed and mean-centered prior to PLS modelling. The reference values where 1 Siemens for MOX sensors, 1 ppm for electrochemical and NDIR sensors, and 1 ou_E/m^3 for odour concentration., The log transformation reduces the dynamic range and linearizes the relationship between $\boldsymbol{X}$ and $\boldsymbol{y}$.

2.3.3. Feature extraction and selection

The pre-processed sensor signals and the olfactometry measurements were used to derive $\boldsymbol{X}$ and $\boldsymbol{y}$, respectively. The columns of $\boldsymbol{X}$ are the concatenation of signal segments (each of duration T min) from the 21 sensors, whereas the rows are the different samples measured with the drone hovering over the selected emission sources. Fig. 5 illustrates with artificially generated data how $\boldsymbol{X}$ and $\boldsymbol{y}$ could look like. Initially, the sensor signals during the whole measurement (i.e. T = 5 min) are included in $\boldsymbol{X}$. This results in a matrix with dimensions 73 (samples) × 945 (features), where 945 is the product of the 21 sensors by the 45 samples/sensor recorded by the IOMS in 5 min. The response vector $\boldsymbol{y}$ (73 × 1) contains the odour concentration (ou_E/m^3) measured by dynamic olfactometry for each sample (odour bag).

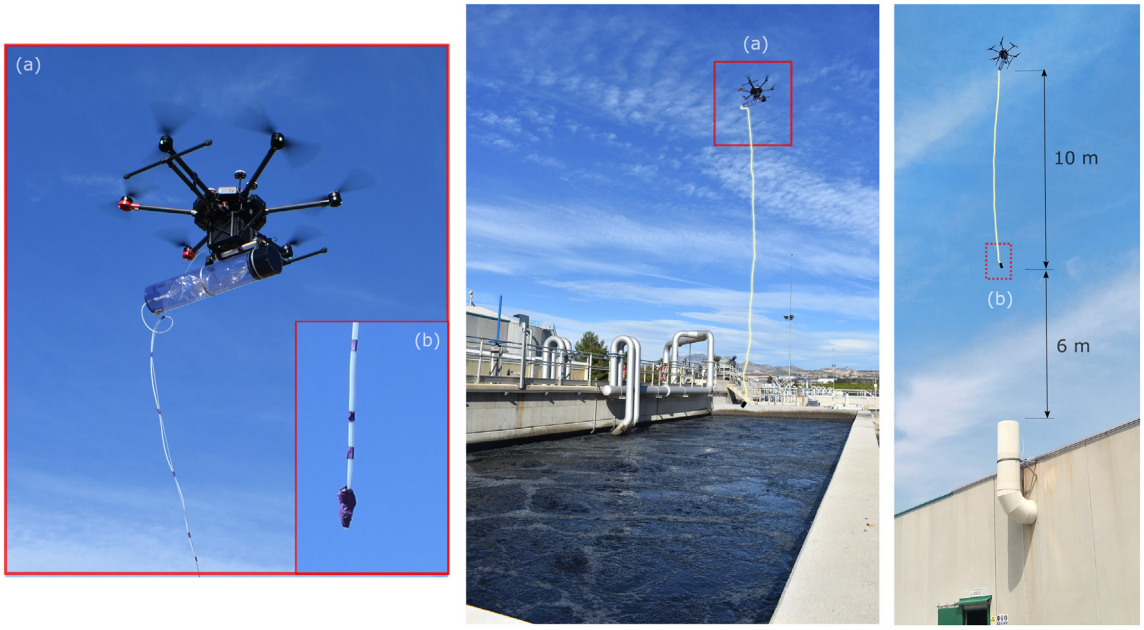

Fig. 4. Photos of the drone during sampling of the bioreactor at 1 m distance (center picture) and the deodorisation chimney at 6 m distance (right picture). The height of the drone in these two examples was 13 m a.g.l. and 25 m a.g.l., respectively. The left picture shows close-up views of (a) the drone and payload and (b) the inlet of the weighted sampling tube.

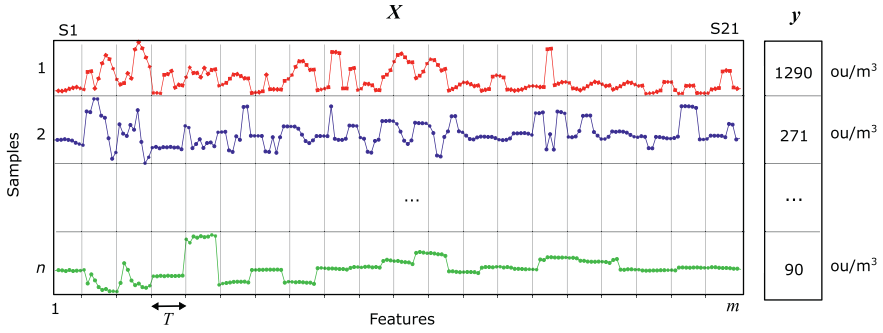

Fig. 5. Schematic representation of the feature matrix X and response vector y (odour concentration). The provided values have been artificially generated for exemplary purposes.

To understand the importance given by the model to the predictors in $\boldsymbol{X}$ and reduce the number of features, we used the variable importance in projection (VIP) method (Chong and Jun, 2005). The idea behind this measure is to accumulate the importance of each predictor j, being reflected by the loading weights, w, for each component of the model. The VIP measure for the jth predictor, v_j, is defined as

$$v_j = \sqrt{p\Sigma_{a=1}^{A}\left[SS_a\left(w_{aj}/\|w_a\|\right)^2\right]/\Sigma_{a=1}^{A}SS_a}, \quad (2)$$

where p is the number of predictors, SS_a is the sum of squares explained by the ath component of the model, and $(w_{aj}/\|w_a\|)^2$ represents the importance of the jth predictor in the ath component. A predictor with a VIP score >1 (one) can be considered important in a PLSR model (Chong and Jun, 2005), therefore we used VIP = 1 as a threshold to discard irrelevant features. The resulting matrix $\boldsymbol{X}_{\mathbf{red}}$ ($n \times m'$) contains the same number of samples than the original matrix $\boldsymbol{X}$ ($n \times m$), but a smaller number of features ($m' < m$).

2.3.4. Calibration model development and validation

Calibration model development encompasses model estimation and complexity control. In the case of a PLS model, complexity control (also known as model selection) means selecting the best number of latent variables (LVs) to ensure the model generalizes well from the training data to data not seen during model development. This model validation must be performed in an independent set of samples that were not used for model development (external validation set). For that, we have chosen a resampled data partition according to a double leave-*one-block*-out cross-validation (CV) scheme in which data from three days (i.e., blocks) are used for model development and the remaining day is used for external (blind) validation (Filzmoser et al., 2009). As illustrated in Table 3, this CV scheme makes the most efficient use of a small dataset because all measurements participate in external validation for unbiased performance assessment. The only practical inconvenience of this approach is that four models are obtained at the end of the process (one model for each validation day), so it is important to verify that the models are comparable with each other before drawing general conclusions. We did that by looking at the regression coefficients β_i and the complexity LV_i of the four models ($i = 1, \ldots, 4$).

Regarding complexity control, we use a "leave one sample out" (LOO) scheme within each of the calibrations sets (Table 4). In each iteration, PLS models with different number of LVs (1, …, 10) are built using all the optimization samples except for one sample that is reserved for estimating the prediction error (internal validation). The process is repeated N times, each time with a different internal validation sample. Once the N iterations are completed, the root mean squared error (RMSE) is computed for the ten models (Eq. (3)):

$$RMSE = \sqrt{\frac{1}{N}\Sigma_{j=1}^{N}\left(y_j - \hat{y}_j\right)^2}, \quad (3)$$

where y_j and $\hat{y}_j$ are the real and predicted odour concentration of the j-th internal validation sample. We call this figure of merit the RMSE in cross validation (RMSECV). The "knee" in the plot of the *RMSECV* versus the number of LVs indicates which could be an optimum number of LVs for that model ($i = 1, \ldots, 4$).

Once the optimal number of LV has been selected, the n PLS models are refit using all calibration samples (see Table 3). These models are then used to predict the odour concentration of the external validation samples. The RMSE of the predictions (i.e. RMSEP) is computed as in Eq. (3). We also computed the bias and 95 % limits of agreement (LoA) as per the Bland-

Table 3
Data splitting for calibration model development (C) and external validation (X).

Model	Day 1	Day 2	Day 3	Day 4
Model 1 (β_1, LV_1)	X	C	C	C
Model 2 (β_2, LV_2)	C	X	C	C
Model 3 (β_3, LV_3)	C	C	X	C
Model 4 (β_4, LV_4)	C	C	C	X

Table 4
Data splitting for model estimation or training (T) and internal validation (V) of Model 1. The letters below each Day indicate the emission source (S: Settler; B: Bioreactor; P: Pretreatment; C: Chimney). Each cell represents all the measurements performed at that emission source in a given day (typically 3 measurements/source in each day, see Table 1).

	Day 2				Day 3				Day 4			
Iteration	S	B	P	C	S	B	P	C	S	B	P	C
1	V	T	T	T	T	T	T	T	T	T	T	T
2	T	V	T	T	T	T	T	T	T	T	T	T
3	T	T	V	T	T	T	T	T	T	T	T	T
…	…	…	…	…	…	…	…	…	…	…	…	…
N	T	T	T	T	T	T	T	T	T	T	T	V

Altman methodology (Bland and Altman, 1999). The Bland-Altman method was developed to overcome the difficulties in comparing a new measurement technique (e.g., e-nose) with a reference technique that is not free of error (e.g., dynamic olfactometry). A plot of the mean differences between the output of the two measurement techniques versus the average of both measurements allows identification of any systematic difference between the measurements (i.e., fixed bias) or possible outliers. The mean difference is the estimated bias, and the SD of the differences measures the random fluctuations around this mean. It is common to compute 95 % LoA for each comparison, which tells us how far apart measurements by two methods are more likely to be for most samples.

2.4. Odour concentration mapping

An odour concentration map is a spatial representation of the e-nose predictions (ou_E/m^3) in a 2D plane covering an area of interest. Drones provide the possibility to have a dense grid of measurement points over the area of interest from which to estimate chemical maps. The visual inspection of those maps allows identifying the major directions in which the odorant components propagate, and how fast the estimated odour concentration decreases when the drone moves away from the emission sources. We can also observe how the different odour sources interact and how their contributions overlap at specific points of the plant.

As a proof of concept for this functionality, a specific flight over a large area of the plant was performed at the end of the 2nd measurement campaign. For this flight, the drone was equipped only with the IOMS (i.e., without the odour sampling device) to increase the flight time. Using a sweeping flight pattern, the drone scanned a region of approximately 200 × 100 m^2 centered around the secondary treatment (settlers and bioreactors) but also including the pretreatment building and the deodorisation chimney. The drone speed was set to ~0.5 m/s to finish the mapping in a reasonable time (~25 min) and at the same time give enough time for the sensors to react to the sample. The map is built with approximately 225 measurement points (25 min flight × 9 samples/min) spatially distributed over a region of approximately 200 × 100 m^2. This is a resolution of 3 m (0.5 m/s × 6 s/sample).

The altitude of the drone was continuously adjusted to keep the inlet of the sampling system as close as possible to the WWTP infrastructure. To produce a continuous and smooth map, we used a natural neighbor interpolator (Sibson, 1981) based on the Delaunay triangulation (Amidror, 2002). We chose this interpolator because it does not infer trends and will not produce artifacts (e.g., peaks, ridges, or valleys) that are not present in the input data.

3. Results and discussion

3.1. Raw sensor signals

As an illustrative example, Fig. 6 shows the sensor signals during the 1st day of measurements. The vertical red bars indicate the moments in which the odour bags were collected, and the number on top the bars indicates their odour concentration (ou_E/m^3). As can be seen, there is a rich pattern of sensor signals with an intensity and fluctuations that depend strongly on the monitored source, sampling distance, local wind conditions and additional factors as temperature and humidity. The strongest responses of all sensors occurred during close-range sampling of the deodorisation chimney, bioreactor, and sludge hoppers, with peak concentrations of 50–80 ppm NH_3 and >40 ppm H_2S (sensor saturation). Odour concentrations for these measurements ranged from 215 to 7298 ou_E/m^3. Above-background levels of CO, SO_2 and CO_2 were recorded in these sources as well. On the other hand, the settlers and the pretreatment building had the lowest concentration of all measured gases, e.g. <10 ppm of H_2S and NH_3.

We observed a fast decay in gas and odour concentration with increasing distance between the sampling inlet and the emission source. For example, the H_2S and NH_3 peak concentrations recorded at the bioreactor decreased by a factor of 2 for every 1 m increase in sampling height (Fig. 7). A factor of two dilution was also observed in the odour concentration, which decreased from 7298 to 4096 to 1993 ou_E/m^3 when increasing the sampling height from 2 to 3 to 4 m, respectively.

However, it is not always easy to fill an odour bag exactly during a peak in the odour emissions, even with real-time visual feedback from the IOMS signals. As illustrated in Fig. 8, the activation of the odour sampling device can happen during a valley in the emissions. This occurs more frequently in point sources emitting a plume than in area sources because in the former case it may be difficult to keep the inlet of the sampling tube inside the plume during the sampling process. Sudden changes in wind direction not only shift the plume away from the sampling tube, but also make the tube oscillate. When the tube gets out the plume, the concentration sharply drops to the background level and the result is a highly diluted odour sample. In the example of Fig. 8, high NH_3 concentrations of 60–80 ppm were recorded at the deodorisation chimney in certain moments in which the inlet of the sampling tube was positioned inside the plume, however the sampling device was often activated when the tube was outside of the plume (due to wind). This led to unrealistically low odour concentrations of 215 and 431 ou_E/m^3 in some bags. Clearly, the odour concentration would have been much higher if the odour bag was filled slightly earlier or later. Even the sample with 5468 ou_E/m^3 can be considered too diluted if compared with the odour concentration that would have been measured 2 min later, i.e., during the peak of 80 ppm NH_3.

3.2. Feature extraction and selection

An illustrative example of the feature matrix X colored by the odour concentration vector y is shown in Fig. 9. It can be observed that six sensors (H_2S, NH_3, CO, M3, M6 and M7) outstand from the others in terms of signal variance. Not all points along the measurement cycle are equally correlated with the odour concentration. The beginning of the measurement (i.e., when the hovering period just started) typically shows little correlation whereas the second half of the measurement seems to carry more relevant information. The role of the calibration model will be to identify those features (i.e., sensors and measurement points) that exhibit high variance in X correlated with *y*.

Using the VIP scores, we identified the most important features for odour prediction (Fig. 10). As it was expected from previous experience in the analysis of WWTP odours and from the signals shown in Fig. 9, the H_2S and NH_3 sensors are the most relevant for the model. Regarding the other sensors, only the CO sensor and three MOX sensors (M3: TGS 2600 at 4.06 V, M6: TGS 2602 at 3.25 V, and M7: TGS 2602 at 4.06 V) were considered important for odour concentration prediction. This agrees quite well with the results we obtained in our previous study where we used steady-state signals to build the predictive models (Burgués et al., 2021a). The VIP scores also indicate that, for nearly all sensors, the features corresponding to the central 1-min period in which the odour bag is filled (red lines) are important for odour prediction. However, the optimum prediction band is delayed by ~30 s or, equivalently, 5 samples (see insets). This is probably due to the time required to fill the sensing chamber and get stable sensor responses, which we empirically estimated as 30 s (see Fig. 8 in (Burgués et al., 2021a)). Intuitively, this could mean that to fully synchronize the sensor responses with the contents of the odour bags it is not enough to compensate for the sample transport time through the tubing but also for the response time of the sensors and the dynamics of the sensor chamber.

3.3. PLS model optimization

Using only the data from the top-five relevant sensors (H_2S, NH_3, M3, M6 and M7) and the most predictive signal features of the measurement cycle, we optimized the PLSR models as explained in Section 2.3.4. We excluded the CO sensor despite having some of its VIP scores higher than 1. This is because those relevant VIP scores correspond to features located at the end of the measurement cycle, which is not consistent with the

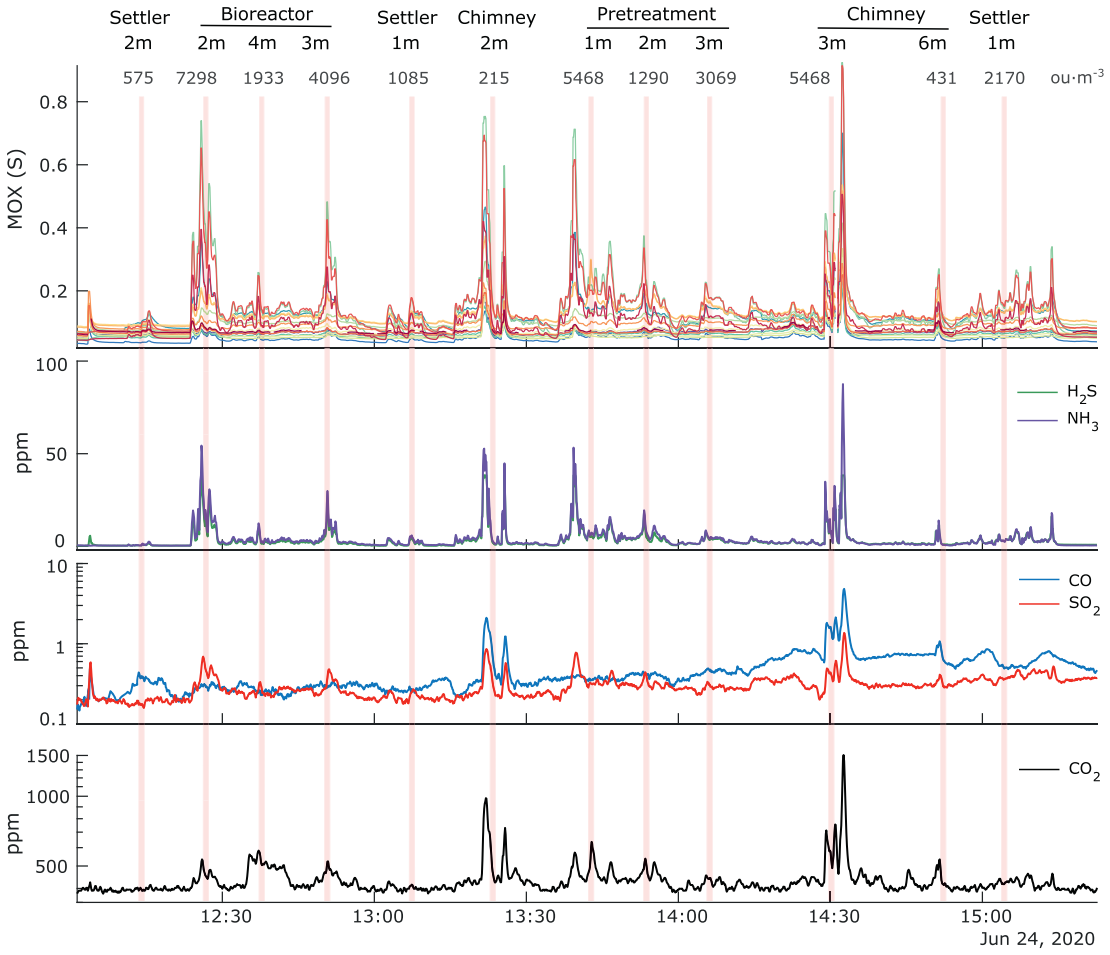

Fig. 6. Gas sensor signals during the 1st experimental day. The vertical shaded bars indicate the sampling moments, and the labels on top of them indicate the source, sampling distance, and odour concentration (ou_E/m^3). The x-axis indicates the timestamp (hh:mm).

pattern observed in the rest of the sensors (relevant features located in the middle of the measurement period) and would require a longer measurement time. The RMSECV vs LV curve (Fig. 11a) had a similar trend for the four PLS models, with increasing RMSECV as more LVs were added to the model. Therefore, 1 LV was selected for all of them. At LV = 1, the RMSECV across the four models ranges between 1.6 and 2.0 (factors), with an average value of 1.8. This means that, on average, the predicted value will be within 1.8 times of the dynamic olfactometry measurement, which is a good result considering that the uncertainty of dynamic olfactometry is close to a factor of 2 (95 % CI). This simple PLS model built with 5 sensors and a reduced feature set improved slightly the results obtained with a full PLS model built with all sensors and all features. The latter required a higher number of LVs (1 or 2 depending on the model) and yielded worse RMSECV values (1.9–2.1).

The fact that the optimum PLS models only require 1 LV deserves additional comments. For example, this could indicate that the sensor array is not sensitive to the odour variability from the different sources; instead, for the PLS algorithm the different odours look like scaled versions of the same pattern. The selected experimental design and model complexity control allowed the PLS algorithm to find a common signature for the

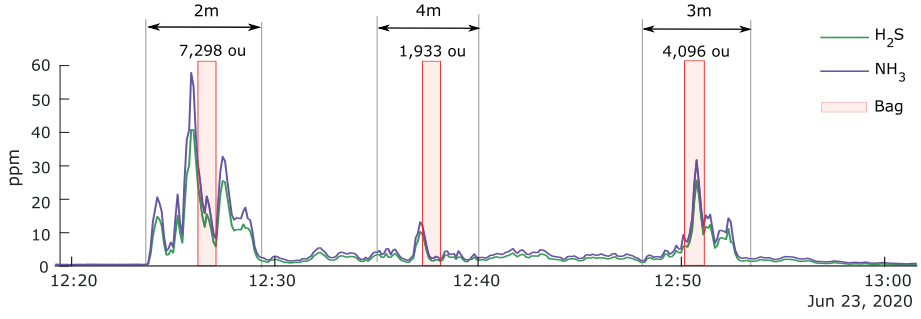

Fig. 7. H_2S and NH_3 sensor signals during measurements above the bioreactor at multiple sampling distances (indicated on top of the figure). The red shaded rectangles and the labels above them indicate the filling of the odour bag and the measured odour concentration (ou_E/m^3), respectively. The x-axis indicates the timestamp (hh:mm). Data corresponds to Day 1.

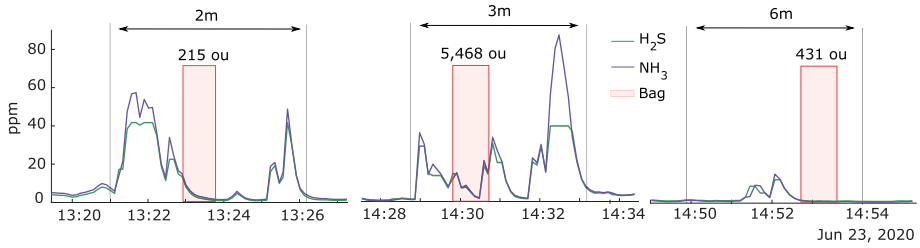

Fig. 8. H_2S and NH_3 sensor signals during measurements above the Chimney at different sampling distances (indicated on top of the figure). The red shaded rectangles and the labels above them indicate the filling of the odour bag and the measured odour concentration (ou_E/m^3), respectively. The x-axis indicates the timestamp (hh:mm). Data corresponds to Day 1.

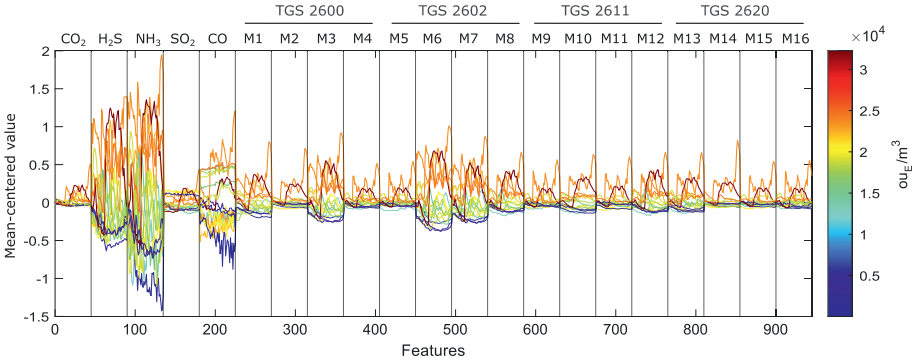

Fig. 9. Feature vectors corresponding to the first three day of measurements, colored by odour concentration (y). The shown signals were mean-centered with respect to the calibration data, after applying the log transformation. The vertical bars separate the features of the different sensors.

WWTP odours that is enough for odour concentration estimation. Regarding the similarity between the four models, Fig. 11b confirms that the four regression vectors are very similar to each other, with Model 4 having a slightly different pattern of coefficients than the other three models. In all cases, the NH_3 sensor seems to have the greatest importance for prediction, followed by the H_2S sensor and the three MOX sensors. The higher importance of the NH_3 sensor versus the H_2S sensor can be unexpected from a theoretical point of view but is reasonable from a pure technical perspective. The reason is that the H_2S sensor used in the e-nose had a lower measurement range (0–40 ppm) than the NH_3 sensor (0–100 ppm), which led to saturation of H_2S sensor in some extreme conditions such as measuring close the deodorization chimney, whereas the NH_3 sensor never saturated in our experiments.

3.4. PLS model validation

The optimized PLS models were validated against external (blind) samples (c.f. Table 3). A scatter plot of the predicted versus real odour concentration reveals a relatively high correlation (rho = 0.86) between the predictions and the reference values (Fig. 12). The four emission sources are predicted with similar errors and the RMSEP is approximately a factor of 2. The bias between the predicted and real

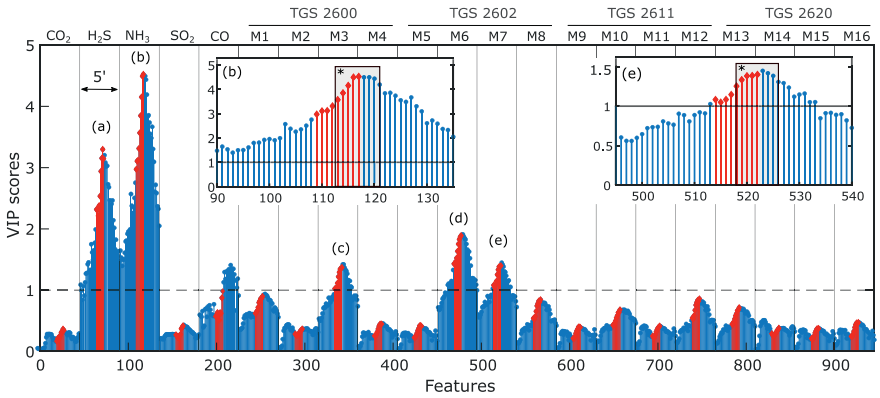

Fig. 10. VIP scores as a function of the feature vector. The x-axis is divided in 21 blocks (sensors) of 45 features. The 45 bars (features) within each block correspond to the sensor response during the 5 min measurement (Fs = 9 samples/min). The red bars highlight the features measured during the 1-min filling of the odour bag. Five relevant sensors with VIP > 1 selected for model building are indicated with letters (a)-(e). The two insets show a close-up view of the VIP scores for the NH_3 and M7 sensors. The vertical rectangle labelled with an asterisk (*) indicates the optimum 1-min measurement band where the VIP scores are maximized.

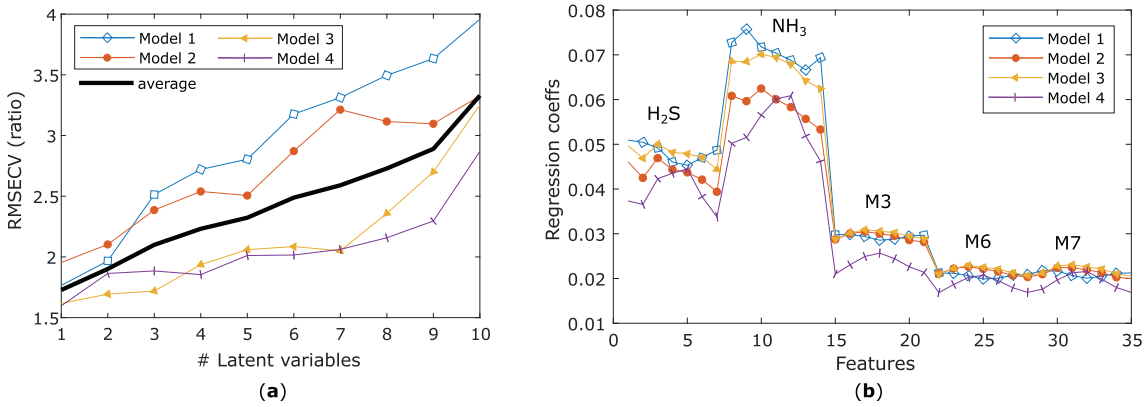

Fig. 11. (a) RMSECV versus number of latent variables and (b) Regression coefficients for the four PLS models (blue: Model 1, red: Model 2, yellow: Model 3, purple: Model 4).

values is negligible and the 95 % limits of agreement (LoA) are [0.25×, 3.91×]. Table 5 compares these results with (a) our previous study in which the IOMS was calibrated and validated in the lab using steady-state signals (Burgués et al., 2021a) and (b) the calibration model developed in the lab with steady-state signals but applied to the validation dataset captured in the current study (transient signals). The best possible predictions are obtained with the calibration model developed and validated in the lab under controlled conditions and using odour bags (1st column of the table, RMSEP = 1.8×). This methodology is however not practical in the intended application. When the steady-state calibration model is fed with transient signals measured in the field (2nd column of the table), the RMSEP degrades from 1.8× to 2.46×, the LoA increases from approximately a factor of 2 to approximately a factor of 6, and the correlation between the predictions and dynamic olfactometry decreases from 97 % to 75 %. Under the same validation conditions, the dynamic calibration model (3rd column of the table) achieves an RMSEP of approximately a factor of 2, a LoA of approximately a factor of 4, and a correlation between the predictions and dynamic olfactometry of 86 %. This confirms the initial hypothesis of the study, i.e. calibration with transient signals measured in the field improves the performance of the drone-based system.

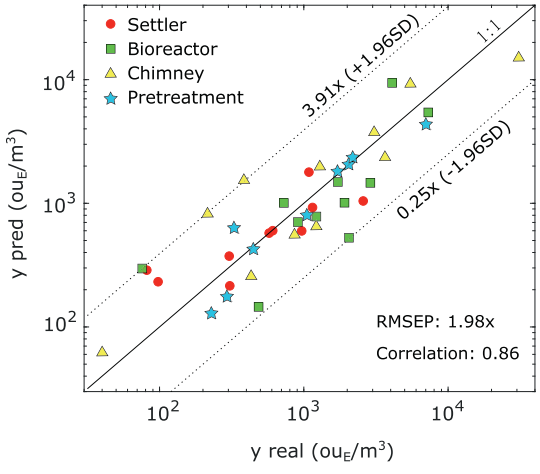

Fig. 12. Validation of dynamic PLS model predictions in external validation (blind) samples measured with the drone. The marker colour indicates the odour source (Settler: red, Biological: green, Chimney: cyan, Desander: purple). The ideal prediction line (1:1) and the upper and lower limits of agreement (LoA) are shown as a dotted line. LoA and RMSEP values are provided as factors (ratios).

3.5. Odour concentration mapping

Fig. 13 shows the interpolated odour concentration map built according to the protocol described in Section 2.4. As expected, the highest odour emissions were concentrated on the southwest side of the plant, which contains the deodorisation chimney and primary treatment elements that receive the influent water, such as the stage A bioreactors and the primary settlers. The northern side of the plant is less odorous because it contains secondary treatment elements that receive cleaner wastewater that has been already pre-treated. This map is shown only for illustrative purposes. An analysis of odour dispersion within the map is out of the scope of this project as the wind information that we collected does not have enough temporal resolution to perform a detailed analysis of odour dispersion.

3.6. Limitations of the study and of the proposed technology

The current version of the SNIFFDRONE systems is probably not robust against harsh environmental conditions. We foresee that in the presence of rain, snow, hail, moderate to strong wind intensity (higher than 30 km/h), freezing temperatures or dust clouds, the system will not operate properly. A more extensive validation is needed to characterize the ruggedness of the system in regards larger excursions of temperature and humidity. Measurements were carried out in summer season because of the higher odour emissions. While the system components are qualified in the range −20 to 60 °C, we expect that the prediction accuracy will degrade in other weather seasons due to temperature cross-sensitivities and differences in chemical composition of the emissions. To characterize the performance of the system in an extended temperature and humidity range we would need to run measurement campaigns in other weather seasons, especially winter, which was out of the scope of this project.

On the other hand, to understand the impact of sensor drift in the system performance, the device performance needs to be assessed during extended periods increasing the time distance between calibration and

Table 5
Comparison of predictive performance between static calibration (RHINOS paper) and dynamic calibration (SNIFFDRONE paper). In all cases, a PLS regression model with 1 LV is used and external (blind) samples are used for validation.

	RHINOS (Burgués et al., 2021a)		SNIFFDRONE
Calibration	Lab (odour bags)	Lab (odour bags)	Field (drone)
Validation	Lab (odour bags)	Field (drone)	Field (drone)
RMSEP	1.8×	2.46×	1.98×
Correlation	0.97	0.75	0.86
Bias	0	0.01	0.01
LoA	[0.41×, 1.97×]	[0.17×, 6.10×].	[0.25×, 3.91×].

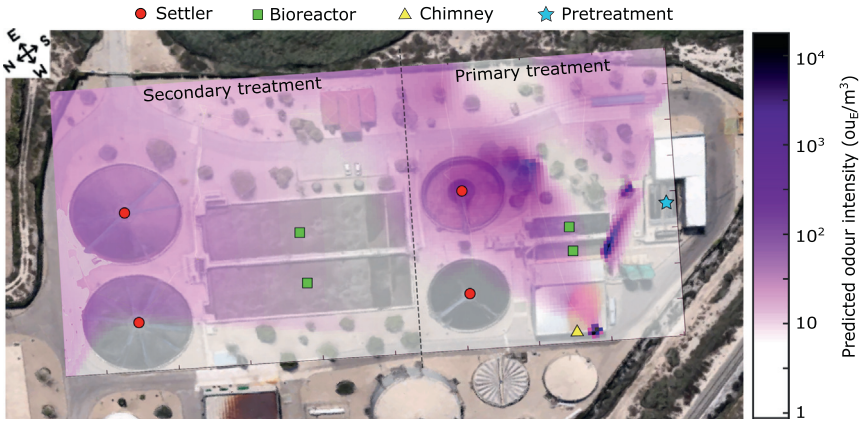

Fig. 13. Interpolated map of odour concentration predictions of a 200 × 100 m^2 region of the plant. The main odour sources are indicated with colored circles. Data was collected with the drone-mounted e-nose during a specific flight at the end of the 2nd campaign. The ambient temperature was 30 °C, relative humidity of 45 %, and wind speed of 12.5 km/h with south-east (SE) direction.

operation. The current system integrates a baseline correction mechanism, but it is not clear from the present study if this measure will be sufficient to provide stability in the long term. Sensitivity drift will require periodic system recalibrations to keep satisfactory performance.

The current calibration protocol is still immature and needs further development. The high cost of each dynamic olfactometry determination limits the number of calibration points, while the high uncertainty associated to EN13725 degrades the quality of the calibration model. Calibrating with few data points necessarily leads to an underrepresentation of the complexity of the problem, most notably ignoring the short- and long-term variability of the emissions due to changing operating conditions, meteorological factors, seasonal trends, etc. Also, the training of non-linear models requires a denser sampling of the plant conditions due to well-known non-linearities in intensity of odour perception. Additionally, as we have already mentioned, the requirement to keep systems calibrated implies to consider not only the initial calibration phase but also the standard operation protocols for system recalibration. The associated cost should be taken into account as well. Finally, the transfer of calibration across units to avoid individual device calibration has not been considered in the present work. Similarly, the transfer of calibration models across plants requires further investigations and it is outside the scope of the present investigation.

Moreover, in its current form, the system assumes that the major contributors to the odour at any measurement location are the sources that were considered in the calibration dataset. This is a common problem in machine learning based prediction models. The algorithm learns to predict the odour concentration from a set of examples. The presence of additional odour sources, not considered in the calibration, will introduce errors in the odour estimation. The magnitude of this error will depend on the intensity of the neglected odour sources and the difference in chemical composition. We should also remark that the performance of the system has been mostly tested in the odour range 100–7000 ou$_E$/m^3. Outside of this range, the system will extrapolate, and errors have not been properly quantified. In other words, odour measurements outside of this range may have relative errors bigger than the stated for the explored range. From the current study, we cannot infer the performance of the system at the location of sensitive receptors, when the odour concentrations are lower than 100 ou$_E$/m^3.

4. Conclusions

In this paper we have shown how a flying electronic nose able to measure odour concentration in real time has been calibrated and validated in a WWTP. The developed prototype worked reliably in the field during several weeks and under slightly different operating and weather conditions. The slight degradation in prediction accuracy as compared to the gold standard (dynamic olfactometry) is more than offset by the extremely low measurement cost, portability of the instrument and immediacy of results, which allows taking many measurements on site and evaluate the results directly in the field. This is an important practical advantage for plant managers, which no longer need to carefully plan olfactometric measurement campaigns and wait several days to get and analyze the results. In contrast, the SNIFFDRONE prototype allows them to routinely take as many odour measurements as needed in almost any location in their plants, get the results immediately and display them in an odour map. This improves their capability to detect and mitigate potential odour problems before they produce a negative impact outside of the plant.

The results presented in this work and their discussion is also a big step forward to understand the challenges associated to machine olfaction in field conditions. While current research has been mostly based in terrestrial robots aiming at the detection of single odorants in simplified exploration areas of limited size, absence of obstacles, and uniform wind conditions (Monroy and Gonzalez-Jimenez, 2018), we carried out field experiments in realistic conditions, i.e. flying over a real WWTP for model development and validation. For the first time, the complexity of this type of operating conditions is addressed. Specifically, we (i) compared two calibration strategies (static and dynamic) for the electronic nose, concluding that dynamic calibration with transient signals measured in flight conditions led to higher prediction accuracy than the traditional steady-state calibration; (ii) analyzed the impact of wind into the sampling system and the sensor signals, revealing a higher impact in point-like sources than in area sources; (iii) discussed the challenges associated to calibrating odour predictive models with real-time sensor signals, proposing a feature extraction and selection method to identify the most promising features along the measurement cycle; and (iv) discussed how the sampling system and the response time of the sensors affects the feature selection, among many other things.

The weakest point of this study is probably the calibration protocol, which is still immature and needs further development and documentation. The high cost and uncertainty of each dynamic olfactometry determination limited the quantity and quality of the calibration points, degrading the quality of the calibration model. Calibrating with few data points leads to an underrepresentation of the complexity of the problem, most notably ignoring the short- and long-term variability of the emissions due to changing operating conditions, meteorological factors, seasonal trends, sensor drift, etc. Also, the training of non-linear models requires a denser sampling of the plant conditions due to well-known non-linearities in intensity of odour perception. Calibrating an instrument with a reference technique that is not free of error hinders the application of standard regression models which assume that the independent variables have been measured

exactly. Additionally, the requirement to keep the system calibrated over time implies to consider not only the initial calibration phase but also: (i) Temporal validation of calibration models (stability and robustness studies); (ii) Periodic re-calibration; (iii) Automatic detection of component failure; (iv) Transfer of calibration models across plants. All these steps need further investigation, and they should be thoroughly documented for future use of the proposed system by plant operators without continuous support from R&D teams.

The high potential demonstrated by the SNIFFDRONE prototype encourages its further development until reaching a pre-commercial stage and extending its application to other sectors in which odour emissions have a strong impact (landfills, farms, composting plants, …). Moreover, the spatially-dense odour measurements that this platform can provide will open new possibilities to fuse sensor data and atmospheric dispersion models(Ravina et al., 2020; Nebenzal et al., 2020). All this can result in a benefit for industrial operators by reducing the capital and operational expenditures (CAPEX and OPEX) associated to odour emission monitoring. This technology can also help to improve the quality of life of people living in proximity to these facilities.

Funding

This research has received funding as third party from the ATTRACT project funded by the EC under Grant Agreement 777222.

Patent

The authors have previously filed a European patent related to the contents of this work with application number EP21382389.1: “Drone to measure odour concentration”.

CRediT authorship contribution statement

Conceptualization, S.M., S.D., L.S. and J.B..; methodology, M.D.E, J.B. and S.M.; sampling campaign design and implementation, S.D., L.S.; software, J.B.; validation, all authors.; formal analysis, J.B.; investigation, J.B.; resources, S.M. and S.D.; data curation, J.B.; writing—original draft preparation, J.B.; writing—review and editing, all authors; visualization, J.B.; supervision, S.M.; project administration, S.M. and S.D.; funding acquisition, S.M. and S.D. All authors have read and agreed to the published version of the manuscript.

Declaration of competing interest

The authors declare the following financial interests/personal relationships which may be considered as potential competing interests: María Deseada Esclapez, Lídia Sauco and Silvia Doñare are employees of Depuración de Aguas del Mediterraneo (DAM). The authors have previously filed a European patent related to the contents of this work with application number EP21382389.1: “Drone to measure odour concentration”.

The funders had no role in the design of the study; in the collection, analyses, or interpretation of data; in the writing of the manuscript, or in the decision to publish the results. Lidia Saúco, Maria Deseada Esclapez and Silvia Doñate are employees of Depuración de Aguas del Mediterráneo (DAM).

Acknowledgments

We would like to acknowledge, the Departament d'Universitats, Recerca i Societat de la Informació de la Generalitat de Catalunya (expedient 2017 SGR 1721); the Comissionat per a Universitats i Recerca del DIUE de la Generalitat de Catalunya; and the European Social Fund (ESF). Additional financial support has been provided by the Institut de Bioenginyeria de Catalunya (IBEC). IBEC is a member of the CERCA Programme/Generalitat de Catalunya. Authors of this report gratefully acknowledge the cooperation of ESAMUR (Entidad Regional de Saneamiento y Depuración de Murcia). We would also like to thank Maria José Ibáñez, Ana Maciá and Pilar Pradas for their support during the field campaigns.

Appendix A. Supplementary data

Supplementary data to this article can be found online at https://doi.org/10.1016/j.scitotenv.2022.157290.

References

Amidror, I., 2002. Scattered data interpolation methods for electronic imaging systems: a survey. J. Electron. Imaging 11, 157–176.
Bax, C., Sironi, S., Capelli, L., 2020. How can odors be measured? An overview of methods and their applications. Atmosphere (Basel) 11, 92.
Bland, J.M., Altman, D.G., 1999. Measuring agreement in method comparison studies. Stat. Methods Med. Res. 8, 135–160. https://doi.org/10.1191/096228099673819272.
Burgués, J., Esclapez, M.D., Doñate, S., Marco, S., 2021. RHINOS: A lightweight portable electronic nose for real-time odor quantification in wastewater treatment plants. iScience 24, 103371. https://doi.org/10.1016/j.isci.2021.103371.
Burgués, J., Esclapez, M.D., Doñate, S., Pastor, L., Marco, S., 2021b. Aerial mapping of odorous gases in a wastewater treatment plant using a small drone. Remote Sens. 13, 1757–1769. https://doi.org/10.3390/rs13091757.
Burgués, J., Esclapez, M.D., Doñate, S., Saúco, L., Marco, S., 2021. Drone-based environmental odour monitoring: SNIFFDRONE. 9th IWA Odour&VOC/Air Emission Conference. Bilbao.
Burgués, J., Hernández, V., Lilienthal, A., Marco, S., 2019. Smelling nano aerial vehicle for gas source localization and mapping. Sensors 19, 478. https://doi.org/10.3390/s19030478.
Burgués, J., Marco, S., 2020. Environmental chemical sensing using small drones: a review. Sci. Total Environ. 748, 141172. https://doi.org/10.1016/j.scitotenv.2020.141172.
Burgués, J., Marco, S., Doñate, S., Esclapez, M.D., Pastor, L., 2020. Drone-based Environmental Odour Monitoring: SNIFFDRONE.
Byliński, H., Gębicki, J., Namieśnik, J., 2019. Evaluation of health hazard due to emission of volatile organic compounds from various processing units of wastewater treatment plant. Int. J. Environ. Res. Public Heal. 16, 1712. https://doi.org/10.3390/IJERPH16101712.
Capelli, L., Sironi, S., Del Rosso, R., 2014. Electronic noses for environmental monitoring applications. Sensors 14, 19979–20007. https://doi.org/10.3390/s141119979.
Carrera-Chapela, F., Donoso-Bravo, A., Souto, J.A., Ruiz-Filippi, G., 2014. Modeling the odor generation in WWTP: an integrated approach review. Water Air Soil Pollut. 225. https://doi.org/10.1007/s11270-014-1932-y.
Chong, I.-G., Jun, C.-H., 2005. Performance of some variable selection methods when multicollinearity is present. Chemom. Intell. Lab. Syst. 78, 103–112.
Devai, I., DeLaune, R.D., 1999. Emission of reduced malodorous sulfur gases from wastewater treatment plants. Water Environ. Res. 71, 203–208. https://doi.org/10.2175/106143098X121842.
Dincer, F., Muezzinoglu, A., 2008. Odor-causing volatile organic compounds in wastewater treatment plant units and sludge management areas. J. Environ. Sci. Health A Toxicol. Hazard. Subst. Environ. Eng. 43, 1569–1574. https://doi.org/10.1080/10934520802293776.
Duisterhof, B.P., Li, S., Burgués, J., Reddi, V.J., de Croon, G.C.H.E., 2021. Sniffy bug: a fully autonomous swarm of gas-seeking Nano quadcopters in cluttered environments. 2021 IEEE/RSJ International Conference on Intelligent Robots and Systems (IROS), pp. 9099–9106.
EN13725, 2022. Stationary Source Emissions - Determination of Odour Concentration by Dynamic Olfactometry and Odour Emission Rate.
Filzmoser, P., Liebmann, B., Varmuza, K., 2009. Repeated double cross validation. J. Chemom. 23, 160–171. https://doi.org/10.1002/cem.1225.
González-Sánchez, A., Revah, S., Deshusses, M.A., 2008. Alkaline biofiltration of H2S odors. Environ. Sci. Technol. 42, 7398–7404. https://doi.org/10.1021/ES800437F.
Hudon, G., Guy, C., Hermia, J., 2000. Measurement of odor intensity by an electronic nose. J. Air Waste Manag. Assoc. 50, 1750–1758. https://doi.org/10.1080/10473289.2000.10464202.
Martí, V., Jubany, I., Pérez, C., Rubio, X., De Pablo, J., Giménez, J., 2014. Human health risk assessment of a landfill based on volatile organic compounds emission, immission and soil gas concentration measurements. Appl. Geochem. 49, 218–224. https://doi.org/10.1016/J.APGEOCHEM.2014.06.018.
Mehmood, T., Liland, K.H., Snipen, L., Sæbø, S., 2012. A review of variable selection methods in partial least squares regression. Chemom. Intell. Lab. Syst. 118, 62–69. https://doi.org/10.1016/J.CHEMOLAB.2012.07.010.
Monroy, J., Gonzalez-Jimenez, J., 2018. Towards odor-sensitive mobile robots. In: Nakamoto, T. (Ed.), Electronic Nose Technologies and Advances in Machine Olfaction. IGI Global, pp. 244–263 https://doi.org/10.4018/978-1-5225-3862-2.ch012.
Munoz, R., Sivret, E.C., Parcsi, G., Lebrero, R., Wang, X., Suffet, I.H.M., Stuetz, R.M., 2010. Monitoring techniques for odour abatement assessment. Water Res. 44, 5129–5149.
Naddeo, V., Zarra, T., Giuliani, S., Belgiorno, V., 2012. Odour impact assessment in industrial areas. Chem. Eng. 30.
Nebenzal, A., Fishbain, B., Kendler, S., 2020. Model-based dense air pollution maps from sparse sensing in multi-source scenarios. Environ. Model. Softw. 128, 104701. https://doi.org/10.1016/j.envsoft.2020.104701.
Ravina, M., Panepinto, D., Mejia Estrada, J., De Giorgio, L., Salizzoni, P., Zanetti, M., Meucci, L., 2020. Integrated model for estimating odor emissions from civil wastewater treatment

plants. Environ. Sci. Pollut. Res. 27, 3992–4007. https://doi.org/10.1007/s11356-019-06939-5.
Sassi, J., Siikanen, S., Höyhtyä, M., 2018. Utilisation of RPAS in Oil and Chemical Detection. Espoo.
Schwarzböck, T., 2012. Market Review on Available Instruments for Odour Measurement.
Serta, R.G., Breda, A., Barreiro, M., Oliveira, J.D., Rodrigues, F.T., 2021. Use of drone to measure odour gases in a refinery plant. Chem. Eng. Trans. 85, 55–60.
Shigaki, S., Fikri, M., Kurabayashi, D., 2018. Design and experimental evaluation of an odor sensing method for a pocket-sized quadcopter. Sensors 18, 3720. https://doi.org/10.3390/s18113720.
Sibson, R., 1981. A brief description of natural neighbour interpolation. In: Barnett, V. (Ed.), Interpreting Multivariate Data. John Wiley & Sons, pp. 21–36.
Sivret, E.C., Wang, B., Parcsi, G., Stuetz, R.M., 2016. Prioritisation of odorants emitted from sewers using odour activity values. Water Res. 88, 308–321. https://doi.org/10.1016/J.WATRES.2015.10.020.
Staerz, A., Roeck, F., Weimar, U., Barsan, N., 2020. Electronic nose: current status and future trends. Surf. Interface Sci. Vol. 9 Appl. Surf. Sci. I 9, 335–379.
Stuetz, R.M., Frechen, F.-B., 2001. Odours in Wastewater Treatment. IWA Publishing.
Szulczyński, B., Namieśnik, J., Gębicki, J., 2017. Determination of odour interactions of three-component gas mixtures using an electronic nose. Sensors 17, 2380. https://doi.org/10.3390/S17102380.
Thomas-Danguin, T., Sinding, C., Romagny, S., El Mountassir, F., Atanasova, B., Le Berre, E., Le Bon, A.-M., Coureaud, G., 2014. The perception of odor objects in everyday life: a review on the processing of odor mixtures. Front. Psychol. 5, 1–18. https://doi.org/10.3389/fpsyg.2014.00504.
Wold, S., Sjöström, M., Eriksson, L., 2001. PLS-regression: a basic tool of chemometrics. Chemom. Intell. Lab. Syst., PLS Methods. 58, pp. 109–130. https://doi.org/10.1016/S0169-7439(01)00155-1.
Yan, L., Liu, J., Jiang, S., Wu, C., Gao, K., 2017. The regular interaction pattern among odorants of the same type and its application in odor intensity assessment. Sensors (Basel) 17. https://doi.org/10.3390/S17071624.
Zarra, T., Naddeo, V., Belgiorno, V., Reiser, M., Kranert, M., 2008. Odour monitoring of small wastewater treatment plant located in sensitive environment. Water Sci. Technol. 58, 89–94.